FEBS Letters 583 (2009) 1017–1022

FEBS Letters
journal homepage: www.FEBSLetters.org

Structure and dynamics of the human muscle LIM protein

Thomas Schallus [a,b], Krisztina Fehér [a,b], Anne S. Ulrich [c], Gunter Stier [a,1], Claudia Muhle-Goll [c,*]

[a] Department of Biomolecular Mechanisms, Max-Planck-Institute for Medical Research, Jahnstrasse 29, 69120 Heidelberg, Germany
[b] Department of Structures and Biocomputing, EMBL, Meyerhofstrasse 1, 69117 Heidelberg, Germany
[c] Karlsruhe Institute of Technology (KIT), Institut für Biologische Grenzflächen (IBG-2), P.O. Box 3640, 76021 Karlsruhe, Germany

ARTICLE INFO

Article history:
Received 22 December 2008
Revised 10 February 2009
Accepted 11 February 2009
Available online 21 February 2009

Edited by Hans Eklund

Keywords:
Cysteine rich protein
NMR
α-Actinin
Telethonin

ABSTRACT

The family of cysteine rich proteins (CRP) comprises three closely homologous members that have been reported to interact with α-actinin. Muscular LIM protein (MLP/CRP3), the skeletal muscle variant, was originally discovered as a positive regulator of myogenesis and is suggested to be part of the stretch sensor of the myofibril through its interaction with telethonin (T-Cap). We determined the structure of both LIM domains of human MLP by nuclear magnetic resonance spectroscopy. We confirm by ^{15}N relaxation measurements that both LIM domains act as independent units and that the adjacent linker regions are fully flexible. With the published structures of CRP1 and CRP2, the complete family has now been structurally characterized.

1. Introduction

The LIM domain motif contains two Zn binding modules or fingers that are closely associated via hydrophobic interactions. It is defined by the consensus sequence $CX_2CX_{16-23}HX_2CX_2CX_2CX_{16-21}CX_{2-3}$(C/H/D). The cysteine rich proteins CRP1, CRP2, and CRP3 or muscular LIM protein (MLP) are composed of two LIM domains separated by a long intervening sequence of more than 50 residues [1] and glycine rich regions adjacent to both LIM motifs. The expression pattern of the CRP protein family is specific for each member [2]. CRP1 is mostly found in smooth muscle tissue, CRP2 in arteries and fibroblasts, and MLP (CRP3) is dominant in striated muscle (cardiac and skeletal), where it is mainly located in the Z-disc, which constitutes the lateral boundary between adjacent sarcomeres, the contractile units of the muscle cell [3–5]. CRP proteins seem to shuttle between the cytoskeleton and the nucleus and thus are postulated to be involved in cell proliferation regulation [6–8]. The nuclear form of MLP was shown to regulate the muscle MyoD transcription factor family [9] and act as a positive regulator of myogenesis [6].

In the sarcomer, MLP is involved in interactions to both α-actinin [10] and βI-spectrin [11], a costameric protein in striated muscle cells, which attributes to MLP a linking role between the contractile apparatus and the plasma membrane. A recent report links MLP to the calcineurin-NFAT signaling pathway [12]. Among other results it was shown that MLP and calcineurin could be coimmunoprecipitated in an apparent dosage dependent way. A central role may play telethonin, a ligand of titin's first two Ig domains Z1Z2, that interacts with MLP and with calsarcin1, another hypothesized member of that pathway [13]. Thus, MLP emerges as a key player linking the contractile apparatus to the plasma membrane and signal transduction pathways in response to mechanical stress.

The structures of the LIM domains of CRP1 and CRP2 have been determined by NMR [14–17]. Here, we present the structural characterization of the third member of this group, MLP.

2. Materials and methods

2.1. Cloning, expression and purification of MLP, N-terminal LIM domain of MLP (LIM1), C-terminal LIM domain of MLP (LIM2)

All constructs for human MLP, LIM1 and LIM2 were cloned into a modified pET-21d vector (Novagen) that contains an N-terminal His_6-tag fused to thioredoxin removable through cleavage with TEV protease. Several constructs spanning the first (LIM1) or

Abbreviations: CRP, cysteine rich protein; HSQC, heteronuclear single quantum coherence; LIM1, N-terminal LIM domain of MLP; LIM2, C-terminal LIM domain of MLP; MLP, muscular LIM protein; NOE, nuclear overhauser effect; NOESY, nuclear overhauser enhancement spectroscopy; hetNOE, heteronuclear NOE; RMSD, root mean square deviation.

* Corresponding author. Fax: +49 721 608 4823.
E-mail address: claudia.muhle@kit.edu (C. Muhle-Goll).
[1] Present address: Department of Biomolecular Mechanisms, Max-Planck-Institute for Medical Research, Jahnstrasse 29, 69120 Heidelberg, Germany.

0014-5793/$36.00
doi:10.1016/j.febslet.2009.02.021

second (LIM2) LIM domain with adjacent linker sequences were subcloned from the MLP vector by PCR. The LIM1 construct employed for NMR studies started with the native sequence, in which the second codon encoding for P was replaced by A for cloning reasons, and stopped at position 85 for LIM1. LIM2 comprised residues 109–194. Details about the cloning and purification have been published elsewhere [18].

2.2. NMR experiments

Spectra were acquired at 22 °C in 20 mM potassium phosphate buffer pH 6.8, 150 mM KCl (LIM1, MLP) or 20 mM Tris buffer, pH 7.2, 150 mM KCl (MLP, LIM2). Details about the assignment have been published elsewhere [18]. For structure determination of LIM1 and LIM2, ^{15}N-heteronuclear single quantum coherence (HSQC)–nuclear overhauser enhancement spectroscopy (NOESY) and ^{13}C-HMQC-NOESY spectra with 80 ms mixing times were recorded on a BRUKER DRX500 spectrometer equipped with a cryoprobe. Data were processed with NMRPIPE [19] and analyzed using NMRVIEW [20].

2.3. Structure calculation

Structures were calculated with ARIA1.2/CNS [21] on the basis of the experimentally derived Nuclear Overhauser Effect (NOE) restraints. Additional dihedral restraints derived from TALOS [22] analysis of the chemical shifts and hydrogen bonds identified on the basis of characteristic NOE patterns (Table 1) were added. Initial rounds of refinements revealed the general fold and the zinc coordination, yet NOE data alone were not sufficient to define the tetrahedral zinc coordination geometry. In the final refinement, distance restraints were added for the Zn–S^{γ} (1.8–2.8 Å) and Zn–$N^{\delta1}$ (1.5–2.5 Å) bonds as well as between the S^{γ} and S^{γ} atoms or S^{γ} and $N^{\delta1}$ atoms. Experimental distance restraints were not violated through this procedure. In the last iteration 200 structures were generated of which 100 were further refined in a shell of water [23]. For the water refinement, the artificial distance restraints were omitted. Instead, the Zn coordination geometry was defined by bonds (Zn–S^{γ} 2.3 Å; Zn–$N^{\delta1}$ 2.0 Å) and angles (109.5° for S^{γ}–Zn–S^{γ}, $N^{\delta1}$–Zn–S^{γ}, Zn–S^{γ}–C^{β} and 120° for Zn–$N^{\delta1}$–C^{β} angles, respectively). The water-refined structures were examined with PROCHECK [24]. Figures were prepared with MOLMOL [25].

2.4. ^{15}N relaxation

Longitudinal and transverse relaxation times as well as heteronuclear NOE were measured at 500 MHz at 20 °C. Protein concentrations were 0.4 mM for LIM1, 0.35 mM for LIM2 and 0.2 mM for MLP. Relaxation delays for T1 were varied between 10.8 ms and 1155.6 ms [26]. T_2 of backbone amide ^{15}N was obtained from $T_{1\rho}$ [27] measurements where a spinlock field strength of 2000 Hz was applied. The $T_{1\rho}$ decay was sampled at relaxation delays between 10 ms and 350 ms with one duplicate point to test for instabilities. The heteronuclear NOE was determined as the signal

Table 1
Structural statistics of LIM1 and LIM2.

	⟨SA-LIM1⟩[a]	⟨SA^{watref}LIM1⟩[a]	⟨SA-LIM2⟩[b]	⟨SA^{watref}LIM2⟩[b]
(A) Number of structural restraints				
All NOE (unambiguous/ambigious)	1277/0		916/0	
Intraresidual	517		430	
Sequential ($\|i-j\|=1$)	218		178	
Medium-range ($1<\|i-j\|\leqslant 4$)	117		74	
Long-range ($\|i-j\|>4$)	425		234	
Dihedral angles $\phi\varphi$	34/34		26/26	
Hbonds	15		14	
(B) RMSD (Å) from experimental restraints[c]				
All distance restraints	0.008 ± 0.001	0.015 ± 0.001	0.007 ± 0.002	0.019 ± 0.002
Dihedral angles[d]	0.65 ± 0.07	0.48 ± 0.1	0.28 ± 0.08	0.5 ± 0.2
(C) Coordinate precision (Å)[e]				
N, C^{α}, C′	0.46 ± 0.17	0.75 ± 0.15	0.88 ± 0.2	1.06 ± 0.23
All heavy atoms	1.11 ± 0.16	1.40 ± 0.19	1.75 ± 0.27	1.92 ± 0.30
(D) Structural quality[f]				
Bad contacts	1.2 ± 1.2	0.0 ± 0.0	0.75 ± 1.07	0.0 ± 0.0
Ramachandran plot				
Residues in most favored region (%)	69.8 ± 2.0	80.5 ± 2.9	75.3 ± 3.9	80.7 ± 3.4
Residues in additionally allowed region (%)	24.9 ± 2.2	14.7 ± 3.2	22.8 ± 4.2	16.4 ± 3.3
RMSD (Å) (N, C^{α}, C′)				
MLP vs qCRP1		2.43		1.92
MLP vs cCRP2		3.08		3.69
cCRP1 vs qCRP2		3.29		2.58
MLP vs ALP-LIM		2.72		3.10
MLP vs CLP36-LIM		1.88		2.71

[a] ⟨SA-LIM1⟩ is an ensemble of 20 lowest-energy solution structures (out of 200 calculated) of the MLP-LIM1 domain before water refinement, ⟨SA^{watref}LIM1⟩ is the ⟨SA-LIM1⟩ ensemble after refinement in a shell of water [18]. The CNS E_{repel} function was used to simulate van der Waals interactions with an energy constant of 25 kcal mol^{-1} Å^{-4} using "PROLSQ" van der Waals radii; RMSD for bond length, bond angles and improper dihedral angles are 0.0023 (±0.0001) Å, 0.426 (±0.012)° and 0.365 (±0.015)° before and 0.0055 (±0.0002) Å, 0.782 (±0.043)° and 2.15 (±0.21)° after water refinement. 1 kcal = 4.18 kJ.

[b] ⟨SA-LIM2⟩ is an ensemble of 20 lowest-energy solution structures (out of 200 calculated) of the MLP-LIM2 domain before water refinement, ⟨SA^{watref}LIM2⟩ is the ⟨SA-LIM2⟩ ensemble after refinement in a shell of water [18]. RMSD for bond length, bond angles and improper dihedral angles are 0.0023 (±0.0001) Å, 0.426 (±0.012)° and 0.365 (±0.015)° before and 0.0055 (±0.0002) Å, 0.782 (±0.043)° and 2.15 (±0.21)° after water refinement. 1 kcal = 4.18 kJ.

[c] Distance restraints were employed with a soft square-well potential using an energy constant of 50 kcal mol^{-1} Å^{-2}. For restraining the zinc coordination 20 distance restraints per domain were applied as described in materials and methods. No distance restraint in the ⟨SA-LIM1⟩[a] and ⟨SA-LIM2⟩[b] was violated by more than 0.2 Å.

[d] Dihedral angle restraints derived from TALOS [19] were applied to ϕ, ψ backbone angles using energy constants of 200 kcal mol^{-1} rad^{-2}.

[e] Coordinate precision is given as the Cartesian coordinate r.m.s. deviation of the 20 lowest-energy structures in the NMR ensemble with respect to their mean structure for residue 7–66 ⟨SA-LIM1⟩ and residue 119–176 ⟨SA-LIM2⟩.

[f] Structural quality was analyzed using PROCHECK [21].

intensity ratio of the H_N/N crosspeaks with and without ^1H saturation. All experiments were recorded in an interleaved manner [28]. The water signal was suppressed with a combination of the water-flip-back and the WATERGATE scheme in all cases. The model-free analysis was carried out with the program Tensor2 [29] for LIM1 and LIM2.

3. Results

3.1. Structure determination of LIM1 and LIM2

The superposition of $^1H^{15}N$ HSQC spectra of full-length human MLP with those of the isolated domains, LIM1 and LIM2, shows that corresponding peaks match each other perfectly well, except for residues at the C-terminus of LIM1 which sense the different chemical environment if the C-terminus is elongated (Supplementary Fig. S1). The remaining peaks in the spectrum of MLP mostly resonate in the central unresolved region, which is characteristic for residues in non-structured parts. We had problems to stably express large quantities of full-length MLP, which was prone to degradation and subsequent precipitation in our hands. Thus, we decided to concentrate for structural work on the LIM domains. Trimming of the C-terminal linker to just the glycine rich region altered the position of several peaks in the spectrum in comparison to full-length MLP. Therefore, we decided to use a construct covering the entire C-terminus of MLP for LIM2 and a comparable sequence range for LIM1 because their peak positions corresponded to those of full-length MLP. We used the native N-terminus for LIM1 and residue 109 as the start for LIM2.

Complete chemical shift assignment was achieved for LIM1 and for almost 90% of LIM2. Resonances of residues 1–6, 113–118, as well as those of several residues in the first and second glycine rich region and the adjacent linker (AA72–83, 179–187) were line-broadened but could be assigned in the triple resonance experiments. Residues 109–112, 183–184 and some residues within the structured part of LIM2 were broadened beyond detection (AA 136,137,143,156,163). Torsion backbone angles derived from the chemical shifts predicted all parts of the inter-domain linker including the glycine rich region, the N-terminus and the C-terminal 20 residues to be unstructured, a fact which was corroborated by the lack of NOEs for these residues. A comparison with triple resonance experiments of MLP revealed that those spectra essentially superimposed as was already shown for the ^{15}N HSQC spectra confirming that the two LIM domains are structurally unrelated.

The solution structures of LIM1 and LIM2 (Fig. 1; experimental restraints and structural statistics are summarized in Table 1) both show the canonical LIM domain fold of two Zn fingers. The structured parts terminate with α-helices just before the start of the immediate adjacent unstructured glycine rich regions. The similarity of the LIM domains is reflected by the pairwise root mean square deviation (RMSD) (N,C^{α},C') of 2.82 Å over the structured region.

3.2. Dynamics

^{15}N relaxation data, sensitive reporters of molecular motion, were obtained for LIM1, LIM2 and compared with those of MLP (Fig. 2). Residues of the unassigned linker were omitted from the analysis of the full-length MLP. All non-structured parts encompassing the glycine rich regions show lower than average R_2 values, reduced or negative heteronuclear NOE (hetNOE) values and low Lipari-Szabo order parameters S^2 (S^2 describes the angular motion for each residue) confirming the high flexibility of these regions in all three constructs. Data obtained for the isolated domains correspond to the values measured for the domains within the full-length protein and corroborate the notion that the two domains act as independent units. The average R_1 value of LIM1 (1.9 Hz) is lower than in LIM2 (2.3 Hz), whereas the average R_2 value (9.8 Hz) of LIM1 is higher than in LIM2 (8.9 Hz) in the isolated domains as well as the full-length protein. The global correlation time, fitted from a set of rigid residues for each domain assuming isotropic tumbling was slightly higher for LIM1 (7.2 ns) than for LIM2 (6.2 ns). This suggests that LIM2 is more flexible as is also reflected by the average hetNOE value of 0.63 (LIM2) vs 0.72 (LIM1). Taking into account all data simultaneously, we fitted a correlation time of 6.9 ns for MLP, which is just the average of the isolated domain values, whereas a rigid protein of 21 kDa would yield a correlation time of ~14 ns. The correlation time is likewise incompatible with dimer formation, because this would manifest itself by a higher τ_c and a higher degree of anisotropy. Together

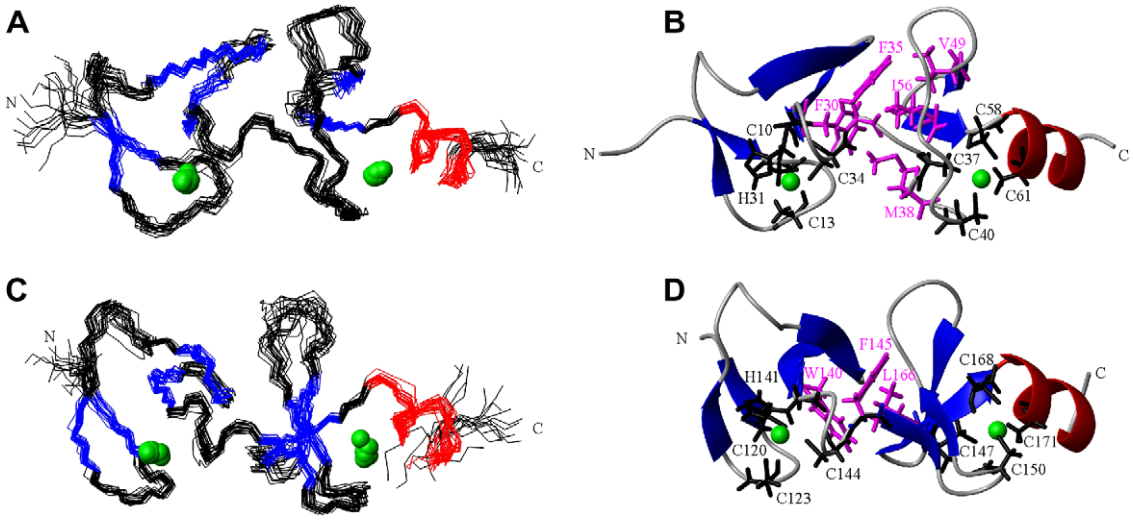

Fig. 1. (A and C) Ensemble of the twenty lowest-energy structures (out of 200 calculated) of the (A) LIM1 domain (residues 6–67) and (C) LIM2 domain (residues 119–176). Secondary structure elements are colored in red and blue for α-helices and β-strands, respectively. The zinc atoms are shown as green spheres. (B and D) Ribbon representation of the MLP–LIM1 and LIM2 domains. Side-chain residues coordinating the zinc atoms are shown in black. Hydrophobic residues that determine the orientation of the Zn fingers are depicted in magenta.

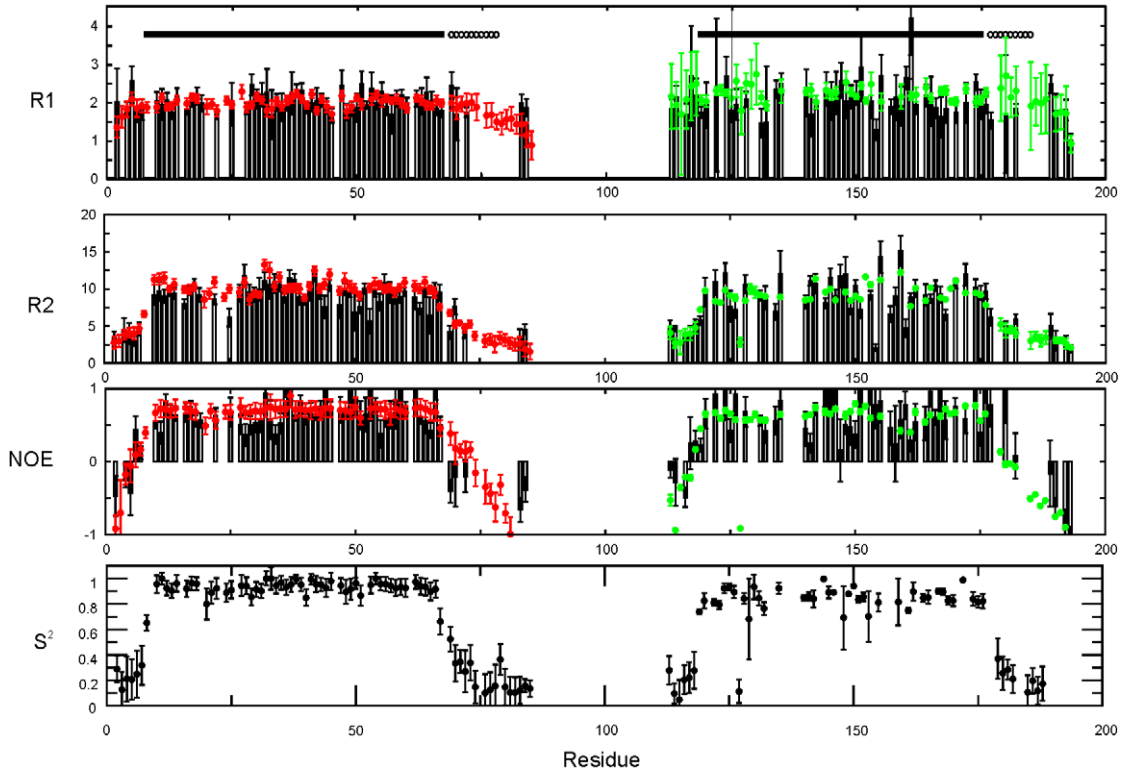

Fig. 2. ^{15}N relaxation data (R1, R2 and hetNOE) for MLP, LIM1 and LIM2. The values of MLP are given as bars. The values of LIM1 and LIM2 are superimposed as red and green circles. Below, the order parameters S^2 derived from Lipari-Szabo model free analysis are illustrated for LIM1 and LIM2. The extension of the LIM domains and the glycine rich domains are shown above the diagram.

with the lack of anisotropy this suggests that the three constructs are tumbling on a similar timescale in spite of the size difference. This demonstrates that the LIM domains do not interact with each other, but are independent domains, as the good agreement between the spectra of the individual LIM domains and that of full-length MLP already suggested.

3.3. Comparison with CRP1 and CRP2

A pairwise comparison of LIM1 and LIM2 with the corresponding LIM domains of chicken CRP1 [15] (1B8T) and quail CRP2 [16,17,30] (1IBI) reveals that despite the well-characterized structures of each LIM domain and the high sequence homology within the LIM1 domains and the LIM2 domains, the RMSDs within one group are of the same order of magnitude as the one obtained between LIM1 and LIM2 domains (Table 1). Moreover, sequentially unrelated LIM domains like the fourth LIM domain from ALP2 (1WIG) and the LIM domain of the PDZ-LIM protein CLP36 (1x62) have comparable RMSDs to LIM1 or LIM2 despite their low sequence homology (Table 1, Supplementary Fig. S2). The large RMSD value for the LIM domains arises mainly from the different relative orientations of the two Zn fingers (Fig. 3A–C).

These are connected through a network of hydrophobic interactions, which is well-defined within each domain. The arrangement of the motifs apparently depends on subtle changes (Fig. 3D). Mainly, a conserved isoleucine or leucine of the second finger (LIM1: Ile56; LIM2: Leu166) can interact with either of two aromatic residues (LIM1: Phe30 and Phe35; LIM2: Trp140 and Phe 145) in the first finger leading to a corresponding rotation of the second Zn finger. This structural variation cannot be attributed to ambiguous or lack of relevant distance restraints because these amino acids are quite well-defined (Table 1).

4. Discussion

In this study we have determined the structure and dynamics of human MLP. With the previously determined structures of chicken CRP1 [15] and quail CRP2 [16,17,30], structures of all three members of the CRP family are thus available and now can be compared.

In the studies on chicken CRP1 and quail CRP2 or their isolated LIM domains structural information could only be retrieved for the folded part of the domains. Residues at the N- and C-termini outside the canonical LIM domain region of CRP1 and CRP2 could not be assigned probably due to exchange phenomena that cause line-broadening beyond detection. Even though some residues experienced a similar phenomenon in the present study, most of the residues of MLP could be assigned [18]. The deviant behavior of MLP in this respect could not have been predicted *a priori*, as sequence identity is high among the members of the CRP family [2] and would have suggested almost identical structural features.

A possible explanation may be that differences in the extent of the various domain assignments reflect rather the intrinsic conformational plasticity of the LIM domains than real structural differences [30–32]. Konrat and coworkers were able to identify correlated motions between the Zn fingers of qCRP2-LIM2 [30] demonstrating that LIM domains are indeed flexible entities. The superposition of the available structures of LIM domains reveals that the highest variability lies in the mutual orientation of the Zn fingers (Fig. 3). Thus, subtle changes in the amino acid composition of the interface and more or less extended interfaces between Zn fingers 1 and 2 appear to lead to various degrees of flexibility. Into this line fits the fact that we find some residues within LIM2 to be exchange-broadened which is generally interpreted as a sign of mobility.

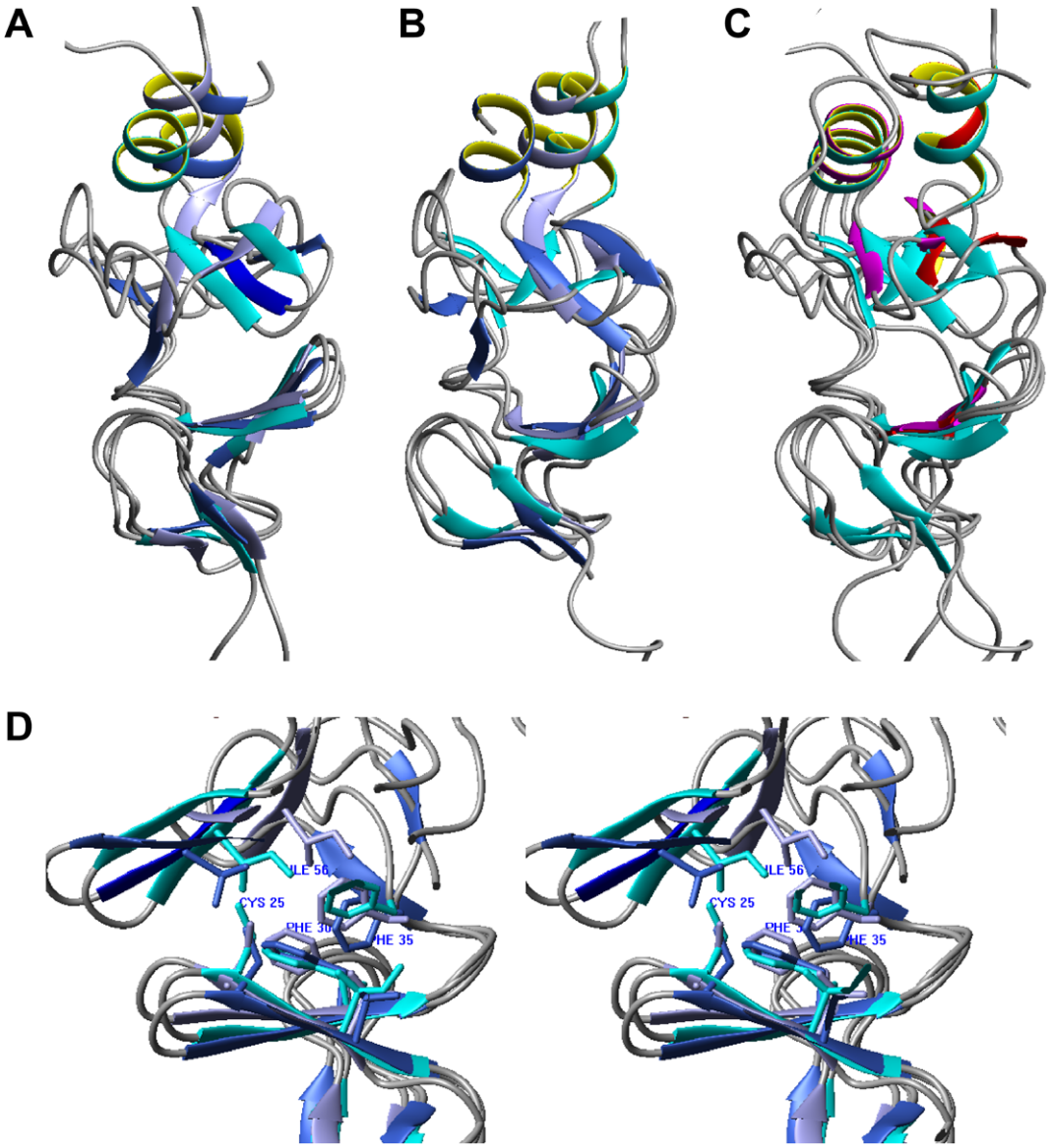

Fig. 3. Structural comparison. The LIM domains are superimposed onto the first Zn finger. β-sheets and α-helices are depicted for clarity. (A) LIM1 of MLP (cyan), chicken CRP1 (light blue) and quail CRP2 (dark blue); (B) LIM2 of MLP (cyan), chicken CRP1 (light blue) and quail CRP2 (dark blue); (C) MLP-LIM1, MLP-LIM2 (both cyan) and ALP (red) and CLP36-LIM (magenta). (D) Details of the interface between the first and the second Zn finger of LIM1. Coloring as in (A).

CRP proteins have been reported to interact with α-actinin 2 [10] and MLP was shown to additionally bind to telethonin [4]. Our attempts to study the interaction of MLP with telethonin or various constructs derived from α-actinin 2, however, did not yield conclusive results. ^{15}N chemical shift perturbation experiments did not show any signs of interaction to telethonin or telethonin in complex with Z1Z2, the first two Ig domains of titin. The addition of the spectrin-like repeats 1–4 of α-actinin 2 induced disappearance of resonances that belong to the structured part and the adjacent glycine rich regions of either MLP, LIM1 or LIM2 in the ^{1}H^{15}N HSQC spectrum (Supplementary Fig. S3). This is a common phenomenon observed in NMR spectroscopy when a protein binds to a large slowly tumbling molecule, like the α-actinin rod (112 kDa). However, it also occurs upon unspecific binding and without further experiments it cannot be judged whether the interaction is specific.

Through solid phase binding assays, however, we identified weak interactions to both the immediate N-terminus of α-actinin 2 and the spectrin-like repeats 1–4 of α-actinin (Supplementary Fig. S4A and B).

Thus we presumed that we observed mainly unspecific binding events mediated through complementary electrostatic charges as both the spectrin-like repeats 1–4 and the N-terminus of α-actinin 2 are negatively charged whereas MLP is a basic protein.

Until recently, interactions lower than micromolar affinities have been regarded as physiologically insignificant. However, the local enrichment of proteins in localized dense sub-compartments of the cell or in multisubunit complexes may drive such equilibrium to complexation even for K_D values that are lower than 10^{-4} M [33]. MLP was reported to be linked to the first two Ig domains of titin Z1Z2 via the common binding partner telethonin [4] although again we failed to prove the binary interaction by NMR (data not shown). Titin on the other hand interacts with the α-actinin CaM domain through its Z-repeats, which are C-terminally upstream of the Z1Z2 [34,35]. Maybe the close vicinity of the proteins leads to higher order complexes where such low affinities could become important.

PDB Accession Numbers: Coordinates have been deposited with the pdb data bank under the Accession Numbers: 2O10 (LIM1) and

2O13 (LIM2). BMRB Accession Number (chemical shift assignment): 15059.

Acknowledgments

The α-actinin plasmid was a gift of Prof. K. Djinovic-Carugo, university of Vienna. Special thanks go to Dr. C. Edlich for initial help with NMR data acquisition and Prof. M. Sattler for access to the spectrometers. C.M.-G. acknowledges support by an Emmy Noether-fellowship of the DFG (Mu-1606-1).

Appendix A. Supplementary data

Supplementary data associated with this article can be found, in the online version, at doi:10.1016/j.febslet.2009.02.021.

References

[1] Weiskirchen, R., Pino, J.D., Macalma, T., Bister, K. and Beckerle, M.C. (1995) The cysteine-rich protein family of highly related LIM domain proteins. J. Biol. Chem. 270, 28946–28954.
[2] Louis, H.A., Pino, J.D., Schmeichel, K.L., Pomiès, P. and Beckerle, M.C. (1997) Comparison of three members of the cysteine-rich protein family reveals functional conservation and divergent patterns of gene expression. J. Biol. Chem. 272, 27484–27491.
[3] Arber, S., Hunter, J.J., Ross Jr., J., Hongo, M., Sansig, G., Borg, J., Perriard, J.C., Chien, K.R. and Caroni, P. (1997) MLP-deficient mice exhibit a disruption of cardiac cytoarchitectural organization, dilated cardiomyopathy, and heart failure. Cell 88, 393–403.
[4] Knöll, R., Hoshijima, M., Hoffman, H.M., Person, V., Lorenzen-Schmidt, I., Bang, M.L., Hayashi, T., Shiga, N., Yasukawa, H., Schaper, W., McKenna, W., Yokoyama, M., Schork, N.J., Omens, J.H., McCulloch, A.D., Kimura, A., Gregorio, C.C., Poller, W., Schaper, J., Schultheiss, H.P. and Chien, K.R. (2002) The cardiac mechanical stretch sensor machinery involves a Z disc complex that is defective in a subset of human dilated cardiomyopathy. Cell 111, 943–955.
[5] Zolk, O., Caroni, P. and Bohm, M. (2000) Decreased expression of the cardiac LIM domain protein MLP in chronic human heart failure. Circulation 101, 2674–2677.
[6] Arber, S., Halder, G. and Caroni, P. (1994) Muscle LIM protein, a novel essential regulator of myogenesis, promotes myogenic differentiation. Cell 79, 221–231.
[7] Arber, S. and Caroni, P. (1996) Specificity of single LIM motifs in targeting and LIM/LIM interactions in situ. Gen. Dev. 10, 289–300.
[8] Chang, D., Belaguli, N., Iyer, D., Roberts, W., Wu, S., Dong, X., Marx, J., Moore, M., Beckerle, M. and Majesky, M. (2003) Cysteine-rich LIM-only proteins CRP1 and CRP2 are potent smooth muscle differentiation cofactors. Dev. Cell 4, 107–118.
[9] Kong, Y., Flick, M.J., Kudla, A.J. and Konieczny, S.F. (1997) Muscle LIM protein promotes myogenesis by enhancing the activity of MyoD. Mol. Cell Biol. 17, 4750–4760.
[10] Pomiès, P., Louis, H.A. and Beckerle, M.C. (1997) CRP1, a LIM domain protein implicated in muscle differentiation, interacts with α-actinin. J. Cell Sci. 139, 157–168.
[11] Flick, M.J. and Konieczny, S.F. (2000) The muscle regulatory and structural protein MLP is a cytoskeletal binding partner of betaI-spectrin. J. Cell Sci. 113, 1553–1564.
[12] Heineke, J., Ruetten, H., Willenbockel, C., Gross, S.C., Naguib, M., Schaefer, A., Kempf, T., Hilfiker-Kleiner, D., Caroni, P., Kraft, T., Kaiser, R.A., Molkentin, J.D., Drexler, H. and Wollert, K.C. (2005) Attenuation of cardiac remodeling after myocardial infarction by muscle LIM protein-calcineurin signaling at the sarcomeric Z-disc. Proc. Natl. Acad. Sci. U.S.A. 102, 1655–1660.
[13] Frey, N., Barrientos, T., Shelton, J.M., Frank, D., Rütten, H., Gehring, D., Kuhn, C., Lutz, M., Rothermel, B., Bassel-Duby, R., Richardson, J.A., Katus, H.A., Hill, J.A. and Olson, E.N. (2004) Mice lacking calsarcin-1 are sensitized to calcineurin signaling and show accelerated cardiomyopathy in response to pathological biomechanical stress. Nat. Med. 10, 1336–1343.
[14] Perez-Alvarado, G.C., Miles, C., Michelsen, J.W., Louis, H.A., Winge, D.R., Beckerle, M.C. and Summers, M.F. (1994) Structure of the carboxy-terminal LIM domain from the cysteine rich protein CRP. Nat. Struct. Biol. 1, 388–398.
[15] Yao, X., Pérez-Alvarado, G.C., Louis, H.A., Pomiès, P., Hatt, C., Summers, M.F. and Beckerle, M.C. (1999) Solution structure of the chicken cysteine-rich protein, CRP1, a double-LIM protein implicated in muscle differentiation. Biochemistry 38, 5701–5713.
[16] Konrat, R., Weiskirchen, R., Krautler, B. and Bister, K. (1997) Solution structure of the carboxyl-terminal LIM domain from quail cysteine-rich protein CRP2. J. Biol. Chem. 272, 12001–12007.
[17] Kontaxis, G., Konrat, R., Krautler, B., Weiskirchen, R. and Bister, K. (1998) Structure and intramodular dynamics of the amino-terminal LIM domain from quail cysteine- and glycine-rich protein CRP2. Biochemistry 37, 7127–7134.
[18] Schallus, T., Edlich, C., Stier, G. and Muhle-Goll, C. (2007) ^{1}H, ^{13}C, and ^{15}N assignment of the muscular LIM protein MLP/CRP3. Biomol. NMR Assign. 1, 41–43.
[19] Delaglio, F., Grzesiek, S., Vuister, G.W., Zhu, G., Pfeifer, J. and Bax, A. (1995) NMRPipe: a multidimensional spectral processing system based on UNIX pipes. J. Biomol. NMR 6, 277–293.
[20] Johnson, B.A. and Blevins, R.A. (1994) NMR View: a computer program for the visualization and analysis of NMR data. J. Biomol. NMR 4, 603–614.
[21] Linge, J.P., O'Donoghue, S.I. and Nilges, M. (2001) Automated assignment of ambiguous nuclear overhauser effects with ARIA. Method. Enzymol. 339, 71–90.
[22] Cornilescu, G., Delaglio, F. and Bax, A. (1999) Protein backbone angle restraints from searching a database for chemical shift and sequence homology. J. Biomol. NMR 13, 289–302.
[23] Linge, J.P., Williams, M.A., Spronk, C.A., Bonvin, A.M. and Nilges, M. (2003) Refinement of protein structures in explicit solvent. Proteins 50, 496–506.
[24] Laskowski, A., Rullmannn, J.A., MacArthur, M.W., Kaptein, R. and Thornton, J.M. (1996) AQUA and PROCHECK-NMR: programs for checking the quality of protein structures solved by NMR. J. Biomol. NMR 8, 477–486.
[25] Koradi, R., Billeter, M. and Wüthrich, K. (1996) MOLMOL: a program for display and analysis of macromolecular structures. J. Mol. Graph. 14, 51–55.
[26] Farrow, N.A., Muhandiram, R., Singer, A.U., Pascal, S.M., Kay, C.M., Gish, G., Shoelson, S.E., Pawson, T., Forman-Kay, J.D. and Kay, L.E. (1994) Backbone dynamics of a free and phosphopeptide-complexed Src homology 2 domain studied by 15N NMR relaxation. J. Struct. Biol. 113, 35–46.
[27] Massi, F., Johnson, E., Wang, C., Rance, M. and Palmer 3rd, A.G. (2004) NMR R1ρ rotating-frame relaxation with weak radio frequency fields. J. Am. Chem. Soc. 126, 2247–2256.
[28] Kay, L.E., Torchia, D.A. and Bax, A. (1989) Backbone dynamics of proteins as studied by 15N inverse detected heteronuclear NMR spectroscopy: application to staphylococcal nuclease. Biochemistry 28, 8972–8979.
[29] Dosset, P., Hus, J.-C., Blackledge, M. and Marion, D. (2000) Efficient analysis of macromolecular rotational diffusion from heteronuclear relaxation data. J. Biomol. NMR 16, 23–28.
[30] Schuler, W., Kloiber, K., Matt, T., Bister, K. and Konrat, R. (2001) Application of cross-correlated NMR spin relaxation to the zinc-finger protein CRP2(LIM2): evidence for collective motions in LIM domains. Biochemistry 40, 9596–9604.
[31] Konrat, R., Krautler, B., Weiskirchen, R. and Bister, K. (1998) Structure of cysteine- and glycine-rich protein CRP2. Backbone dynamics reveal motional freedom and independent spatial orientation of the lim domains. J. Biol. Chem. 273, 23233–23240.
[32] Kloiber, K., Weiskirchen, R., Krautler, B., Bister, K. and Konrat, R. (1999) Mutational analysis and NMR spectroscopy of quail cysteine and glycine-rich protein CRP2 reveal an intrinsic segmental flexibility of LIM domains. J. Mol. Biol. 292, 893–908.
[33] Vaynberg, J., Fukuda, T., Chen, K., Vinogradova, O., Velyvis, A., Tu, Y., Ng, L., Wu, C. and Qin, J. (2005) Structure of an ultraweak protein-protein complex and its crucial role in regulation of cell morphology and motility. Mol. Cell. 17, 513–523.
[34] Ohtsuka, H., Yajima, H., Maruyama, K. and Kimura, S. (1997) The N-terminal Z repeat 5 of connectin/titin binds to the C-terminal region of α-actinin. Biochem. Biophys. Res. Commun. 235, 1–3.
[35] Sorimachi, H., Freiburg, A., Kolmerer, B., Ishiura, S., Stier, G., Gregorio, C.C., Labeit, D., Linke, W.A., Suzuki, K. and Labeit, S. (1997) Tissue-specific expression and α-actinin binding properties of the Z-disc titin: implications for the nature of vertebrate Z-discs. J. Mol. Biol. 270, 688–695.